Biotechnology Notes 4 (2023) 135–145

Contents lists available at ScienceDirect

Biotechnology Notes

journal homepage: www.keaipublishing.com/en/journals/biotechnology-notes/

Fine-tuning the cell morphology of *Corynebacterium glutamicum* via dual-valve regulation for enhanced hyaluronic acid production

Shuting Yuan [a,b], Yukun Zheng [a,b], Yan Du [a,b], Mingye Song [a,b], Claudia Chen Sun [a,b], Fangyu Cheng [a,b], Huimin Yu [a,b,c,*]

[a] *Department of Chemical Engineering, Tsinghua University, Beijing, 100084, PR China*
[b] *Key Laboratory for Industrial Biocatalysis, Ministry of Education, PR China*
[c] *Center for Synthetic and Systems Biology, Tsinghua University, Beijing, 100084, PR China*

ARTICLE INFO

Keywords:
Morphology engineering
Arabinose-inducible expression system
Engineered *Corynebacterium glutamicum*
Hyaluronic acid

ABSTRACT

Enhanced synthesis of hyaluronic acid (HA) with recombinant *Corynebacterium glutamicum* as production host was achieved in this work. Hyaluronan synthase (HAS), which is a membrane protein acting as a key enzyme in HA biosynthesis, impacts both HA yield and its molecular weight. Cell morphology, which includes size, shape, and surface area, has a large impact on the expression and activity of HAS. Therefore, deliberate regulation of cell morphology holds the potential to enhance HA production. Here, we constructed three modules, namely the transporter module, the morphology tuning module and the HA synthesis module. The transporter module contains a strong constitutive promoter P_{tuf} and arabinose transport protein was used to control the maximum amount of inducer entering the cell, thus reducing excessive cell deformation. The morphology tuning module contains an arabinose-inducible weak promoter P_{BAD} and a cell-division-relevant gene was used to sense intracellular inducer concentrations and achieve different degrees of change in cell size. These two modules worked together, described as a dual-valve regulation, to achieve fine-tuning of cell morphology, resulting in a 1.87-fold increase in cell length and a 2.08-fold increase in cell membrane. When combined with the HA synthesis module, the HA titer reached 16.0 g/L, which was 1.6 times the yield reported in the previous morphology-engineered strain. Hence, for the first time, a morphologically engineered strain resulting in both high cell density and HA titer was constructed.

1. Introduction

Hyaluronic acid (HA) is an important glycosaminoglycan (GAG), comprising alternating D-glucuronic acid (GlcUA) and N-acetyl-D-glucosamine (GlcNAc) monomers linked through β-1,3 and β-1,4 glycosidic bonds. HA is characterized by its remarkable water-retention and moisturizing properties, high viscoelasticity, exceptional lubrication, and excellent biocompatibility, which attributes to its wide applications in cosmetics, clinical medicine, and health care products.[1–3] HA biosynthesis requires the involvement of a variety of enzymes, the most critical being the membrane protein hyaluronan synthase (HAS), a bifunctional glycosyltransferase that synthesizes HA chains using UDP-D-glucuronic acid (UDP-GlcUA) and UDP-N-acetyl-D-glucosamine (UDP-GlcNAc).[4,5] By heterologous expression of HAS, HA synthesis has been successfully achieved in *E. coli*,[6,7] *B. subtilis*,[8,9] *C. glutamicum*,[10–12] and *L. lactis*.[13,14] Currently, the main strategies for enhanced HA production include metabolic engineering, protein engineering, and process engineering.[15,16] A new innovative perspective for improving the performance of HA synthesis is by increasing the expression of HAS by altering the cell membrane though morphological engineering of the host cell.[17]

Cell morphology, which includes size, shape and surface area, plays an important role both in cell growth and production. Morphology engineering refers to achieving changes in cell morphology by regulating the expression of related proteins.[18,19] Proteins that affect cell morphology play important roles in cell division, cytoskeleton maintenance, cell wall synthesis and hydrolyzation.[20] Strategically controlling cell morphology holds great significance in strengthening the synthesis of target products. Thus, for intracellular products, increasing cell volume can effectively provide more space for product synthesis. As shown in literature, overexpressing the cytokinesis inhibitory protein SulA while backfilling the cytoskeletal actin protein MreB changed the cell's

* Corresponding author. Department of Chemical Engineering, Tsinghua University, Beijing, 100084, PR China.
E-mail address: yuhm@tsinghua.edu.cn (H. Yu).

https://doi.org/10.1016/j.biotno.2023.12.003
Received 17 November 2023; Received in revised form 9 December 2023; Accepted 9 December 2023
Available online 11 December 2023

appearance from a rod-shape to an elongated filament, increasing the yield of poly-β-hydroxybutyrate (PHB) by 100%, reaching 8.11 g/L.[21] For the synthesis of products requiring the participation of membrane proteins, increasing the cell membrane area is instrumental for elevating enzyme levels and their activity to enhance production.[22] Previous attempts by Zheng et al. to overexpress the cell-division-relevant gene *ftsZ* in *C. glutamicum* resulted in dumbbell-like enlarged cells, which enhanced single-cell HAS level and HA titer by 2.1-fold and 13.5-fold, respectively.[23] In this work, however, overexpression of *ftsZ* greatly inhibited cell growth, leading to a severe decrease in cell number and overall HA titer. We found that in the recombinant strain, *ftsZ* and *hasAB* (HA-synthesis operon) were both expressed by the same strong inducible promoter P_{tac}, consequently the resulting engineered cell size was hypertrophic, thereby severely inhibiting cell division, then significantly reducing cell density and HA accumulation. Therefore, it is worth investigating whether cell-size engineering through the accomplishment of mild-regulation of cell division and precise control of the cell enlargement degree can impact the overall HA productivity.

In this work, we tried to explore a feasible way to achieve mild-regulation of cell division and fine-tuning of *C. glutamicum* cell size. Hence, we constructed two independent modules, namely the transporter module and the morphology tuning module, which combined together to create an elegant dual-valve regulation strategy via arabinose-based transporter-promoter in *C. glutamicum*. By judiciously regulating the expression of arabinose transporter proteins and cell morphology proteins, cell size was enlarged within a defined range, facilitating enhanced HA synthesis without impeding normal cell growth.

2. Material and methods

2.1. DNA manipulation

DNA electrophoresis, DNA enzyme digestion and ligation, Gibson assembly reaction, and plasmid transformations were performed according to the standard laboratory protocols. Phanta high-fidelity DNA polymerase used in polymerase chain reaction was from Vazyme, China. Plasmid extraction kit and gel extraction kit were from Omega, United States. Gibson assembly reaction kits were from Vazyme, China. QuickCut restriction enzymes were from Takara, China.

2.2. Plasmid and strain construction

The plasmids and strains used in this study are listed in Table 1. The primers used for gene amplifications are listed in Table 2. Plasmid pEC-P_{tac} was the backbone for gene *ftsZ*. Plasmid pk18mobsacB, which is lethal in presence of sucrose, can be used for genome editing via double crossover homologous recombination. Ara gene fragment containing regulatory protein gene *araC*, regulatory protein gene promoter P_c and arabinose promoter P_{BAD} was amplified using prime pEC-Ara-F and pEC-Ara-R. The plasmid backbone was amplified using prime pEC-F and pEC-R from template pEC-AB-*ftsZ*. These two fragments were fused by Gibson assembly reaction, and the resulting plasmid was pEC-AB-P_{BAD}-*ftsZ*. Gene *araE* was synthesized based on known gene sequences by GENEWIZ, Inc. Gene fragment P_{tuf}, ltbR upstream and ltbR downstream were all cloned from *C. glutamicum* ATCC13032 using corresponding prime P_{tuf}-F and P_{tuf}-R, ltbR-up-F and ltbR-up-R, ltbR-down-F and ltbR-down-R. Plasmid pK18mobsacB was double digested using *HindIII* and *XbaI* restriction enzymes. The backbone pK18mobsacB, gene fragment ltbR-up, ltbR-down, P_{tuf}, and *araE* were fused by Gibson assembly reaction, and the resulting plasmid was pk18P_{tuf}-araE.

2.3. Shake flask culture of recombinant C.glutamicum

The seed solution was cultured in LBG medium (NaCl 10 g/L, yeast extract 5 g/L, tryptone 10 g/L, glucose 5 g/L) containing 25 μg/mL kanamycin overnight at 30 °C, 200 rpm.

The seed solution was inoculated with 2.5%v/v inoculum in 50 ml fermentation medium (corn syrup powder: 20 g/L, glucose: 40 g/L, glutamine: 1.5 g/L, $(NH_4)_2SO_4$: 30 g/L, KH_2PO_4: 1 g/L, K_2HPO_4: 0.5 g/L, $MgSO_4{\cdot}7H_2O$: 5 g/L, $FeSO_4{\cdot}7H_2O$: 10 mg/L, $MnSO_4{\cdot}7H_2O$: 10 mg/L, kanamycin: 25 μg/mL) in a 500 ml flask. The culture condition was 30 °C, 200 rpm. 0.3 mM IPTG and 0.15 g L-arabinose were added as inducers after 3 h pH was adjusted to 7.2 every 12 h and 15 g/L glucose was supplemented at 24 h.

Table 1
Plasmids and Strians used in this study.

Plasmids and Strains	Description	References
Plasmids		
pEC-XK99E	$Kana^r$, P_{trc}-MCS, rep from native plasmid pGA1 (GenBank: X90817.2) of *C. glutamicum*	24
pk18mobsacB	$Kana^r$, sacB from *B.subtilis*	25
pEC-P_{tac}-GFP	pEC-XK99E derivate, P_{tac}-gfpuv-Ter	10
pEC-P_{tuf}-GFP	pEC-XK99E derivate, P_{tuf}-gfpuv-Ter	10
pEC-P_{fba}-GFP	pEC-XK99E derivate, P_{fba}-gfpuv-Ter	10
pEC-P_{sod}-GFP	pEC-XK99E derivate, P_{sod}-gfpuv-Ter	10
pEC-P_{gap}-GFP	pEC-XK99E derivate, P_{ga}-gfpuv-Ter	10
pEC-P_{eno}-GFP	pEC-XK99E derivate, P_{eno}-gfpuv-Ter	10
pEC-P_{acn}-GFP	pEC-XK99E derivate, P_{acn}-gfpuv-Ter	10
pEC-P_{pgk}-GFP	pEC-XK99E derivate, P_{pgk}-gfpuv-Ter	10
pEC-P_{groES}-GFP	pEC-XK99E derivate, P_{groE}-gfpuv-Ter	10
pEC-P_{dapB}-GFP	pEC-XK99E derivate, P_{dapB}-gfpuv-Ter	10
pEC-P_{pkfA}-GFP	pEC-XK99E derivate, P_{pkfA}-gfpuv-Ter	10
pEC-P_{dapA}-GFP	pEC-XK99E derivate, P_{dapA}-gfpuv-Ter	10
pEC-P_{ddh}-GFP	pEC-XK99E derivate, P_{ddh}-gfpuv-Ter	10
pEC-P_{zwf}-GFP	pEC-XK99E derivate, P_{zwf}-gfpuv-Ter	10
pEC-P_{mphA}-GFP	pEC-XK99E derivate, P_{mphA}-gfpuv-Ter	10
pEC-P_{recA}-GFP	pEC-XK99E derivate, P_{recA}-gfpuv-Ter	10
pEC-P_{tac}	rep from native plasmid pGA1 (GenBank: X90817.2) of *C. glutamicum*, $Kana^r$, P_{tac}, lacI	23
pEC-AB	pEC-P_{tac} derivate, P_{tac}-hasA-hasB-Ter	23
pEC-AB-*ftsZ*	pEC-P_{tac} derivate, P_{tac}-hasA-hasB-*ftsZ*-Ter	23
pMBAD-hasA-hasB	Plasmid carrying araC-Pc-P_{BAD}-hasA-hasB	Laboratory storage
pEC-P_{tac}-AB-P_{BAD}-*ftsZ*	pEC-P_{tac} derivate, P_{tac}-hasA-hasB-araC-P_{BAD}-*ftsZ*-Ter	This work
pEC-P_{tac}-AB-*ftsZ*	pEC-P_{tac} derivate, P_{tac}-hasA-hasB-*ftsZ*-Ter	This work
pk18-P_{tuf}-araE	pk18mobsacB derivate, harboring ltbR upstream, P_{tuf}, araE and ltbR downstream homologous arm	This work
Strains		
E.coli TOP10	F-mcrAΔ(mrr-hsdRMS-mcrBC) φ80 lacZ ΔM15 Δlac X74 recA1 deoR araD139 Δ(ara-leu) 7697 galU galK rpsl (strR) endA1 nupG	Solarbio
C. glutamicum ATCC13032	Wild type	26
Cg-P_{tuf}-araE	Wild type derivate, pk18P_{tuf}-araE	This work
Cg-P_{tac}-GFP	Wild type derivate, pEC-P_{tac}-GFP, $Kana^r$	10
Cg-P_{tuf}-GFP	Wild type derivate, pEC-P_{tuf}-GFP, $Kana^r$	10
Cg-P_{fba}-GFP	Wild type derivate, pEC-P_{fba}-GFP, $Kana^r$	10
Cg-P_{sod}-GFP	Wild type derivate, pEC-P_{sod}-GFP, $Kana^r$	10
Cg-P_{gap}-GFP	Wild type derivate, pEC-P_{gap}-GFP, $Kana^r$	10
Cg-P_{eno}-GFP	Wild type derivate, pEC-P_{eno}-GFP, $Kana^r$	10
Cg-P_{acn}-GFP	Wild type derivate, pEC-P_{acn}-GFP, $Kana^r$	10
Cg-P_{pgk}-GFP	Wild type derivate, pEC-P_{pgk}-GFP, $Kana^r$	10
Cg-P_{groES}-GFP	Wild type derivate, pEC-P_{groES}-GFP, $Kana^r$	10
Cg-P_{dapB}-GFP	Wild type derivate, pEC-P_{dapB}-GFP, $Kana^r$	10
Cg-P_{pkfA}-GFP	Wild type derivate, pEC-P_{pkfA}-GFP, $Kana^r$	10
Cg-P_{dapA}-GFP	Wild type derivate, pEC-P_{dapA}-GFP, $Kana^r$	10
Cg-P_{ddh}-GFP	Wild type derivate, pEC-P_{ddh}-GFP, $Kana^r$	10
Cg-P_{zwf}-GFP	Wild type derivate, pEC-P_{zwf}-GFP, $Kana^r$	10
Cg-P_{mphA}-GFP	Wild type derivate, pEC-P_{mphA}-GFP, $Kana^r$	10
Cg-P_{recA}-GFP	Wild type derivate, pEC-P_{recA}-GFP, $Kana^r$	10
Cg01	*Cg*-araE derivate, pEC-P_{tac}-AB, $Kana^r$	This work
Cg02	*Cg*-araE derivate, pEC-AB-*ftsZ*, $Kana^r$	This work
Cg03	*Cg*-araE derivate, pEC-P_{tac}-AB-P_{BAD}-*ftsZ*, $Kana^r$	This work

Table 2
Primers used in this study.

Primer	Sequences (5′–3′)
pEC-Ara-F	AAATCAATTATGACAACTTGACGGCTA
pEC-Ara-R	ATGGAGAAACAGTAGAGAGTTGCG
ftsZ-F	CAAAGGAGGACACATATGACCTCACCGAACAACTACCT
ftsZ-R	CCGGAATTCTTACTGGAGGAAGCTGGGTACATC
pEC-F	TAGCCGTCAAGTTGTCATAATTGATTTGTCCTACTCAGGA
pEC-R	ACTCTCTACTGTTTCTCCATACCCGTTTTTTTGGGCTAGA
P_{tuf}-F	GCTCAGATCGTTTAGATCCGAAGG
P_{tuf}-R	TCCTCCTTTTGTATGTCCTCCTGGAC
ltbR-up-F	TATGACATGATTACGAATTCGGAACTGGGTTCGGGGCGGA
ltbR-up-R	GGTACCCAGCTTTTGGAGCGCCTAGGCGCTTTGCT
ltbR-down-F	CGCGTGTAAACCTTGAATTTAGCATTTCACC
ltbR-down-R	AGGTCGACTCTAGAGGATCCATCTTGGCGATAATCGCCAG
dnaE(qRT)-F	ATTTGAAGGCGCACTACGCG
dnaE(qRT)-R	CGGCGAAAGCACTCGAATTCC
ftsZ(qRT)-F	CTCGAAGCAACAATGGACGG
ftsZ(qRT)-R	TTGACATCTTCATCGGAACGC
pEC-test-F	TCGGAAGCTGTGGTATGGCTG
pEC-test-R	TCACTTCTGAGTTCGGCATGGG
araE-test-F	TGAGCGAGGAAGCGGAAGAG
araE-test-R	CGACCTTGTCAAAGGTTGCG

2.4. GFPuv reporter assessment

Promoters were assembled with a UV light-excitable green fluorescent protein (GFP) to evaluate the promoter strengths. Detailed information can be found in our previous study.[27]

2.5. RNA isolation, reverse transcriptase PCR, quantitative real-time PCR (qRT-PCR) assay

The operation of RNA isolation, reverse transcription PCR and quantitative real-time PCR (qRT-PCR) were manipulated according to the previous manual set up in our laboratory.[25] A housekeeping gene, *dnaE,* was chosen to normalize the expression of the target gene *ftsZ*. Primers dnaE(qRT)-F/dnaE(qRT)-R and ftsZ(qRT)-F/ftsZ(qRT)-R were used.

2.6. Cell morphology observation by transmission electron microscope (TEM)

1 ml of fermentation broth was taken and washed twice using PBS buffer, then it was diluted 20 times and dropped on a carbon-coated copper grid for 2 min, filter paper was used to absorb excess liquid droplets. 1 μl sodium phosphotungstate solution was taken and dropped onto the sample to stain for 1 min, and excess liquid droplets were absorbed using filter paper.

2.7. Cell morphology observation by scanning electron microscope (SEM)

1 ml fermentation broth was collected and centrifuged at 13000 rpm for 2 min to get the bacterium. After washing the cells twice with deionized water, 1 mL fixative (2.5 % glutaraldehyde) was added and the mixture was placed in a shaker at 30 °C and 200 rpm for 2 h to fully fix the cell. Cells were harvested and freeze-dried to obtain the dried bacterial powder. An appropriate amount of dried bacterial powder was attached to the conductive adhesive, and the surface was sprayed with gold for a duration of 60 s. Cell morphology was observed using scanning electron microscope (QuanTa 200).

2.8. Microbial number calculation by hemocyte counting plate

Cells were harvested by centrifugation at 13,000 rpm for 3 min from 1 ml fermentation broth and washed twice with deionized water. The harvested cells were then resuspended in 1 ml deionized water and its OD_{600} was measured using a visible light spectrophotometer. After that, the treated fermentation broth was diluted 20-100 times, until the final OD_{600} was 1. 2 μl of the diluted liquid was then taken and evenly spread on the counting area of hemocyte counting plate, after being dried at room temperature, 100 μl dye was added to stain the cell for 3 min. The dye was gently washed off with deionized water and the cells were dried at room temperature. 20 μl of pine oil were then added on the plate, the cell number was calculated using 100× objective lens by NIKON Eclipse 50i.

2.9. HA titer and single cell HA synthesis determination

3 ml anhydrous ethanol was added to 1 ml of the fermentation broth and stored at 4 °C for 2 h. After being centrifuged at 10,000 rpm for 3 min, the supernatant is removed and the tube is inverted at room temperature for 1 h to dry the precipitate. Finally, 1 ml deionized water was added and the precipitate was fully resuspended. The preliminary purified HA product was obtained by centrifugation at 10,000 rpm for 1 min.

The HA titer was determined by the modified CTAB method.[25,26]

Single cell HA synthesis was calculated by the following formulate:

$$Single\ cell\ HA\ synthesis = \frac{HA\ titer}{OD_{600} \times cell\ number\ per\ OD}$$

2.10. Quantitative analysis of HA synthesis pathway metabolites

Liquid mass spectrometer (AB SCIEX QTRAP 6500) was used for the quantitative analysis. Pretreatment was completed as follows: 1 ml fermentation broth was taken and centrifuged at 13,000 rpm for 3 min, the supernatant was discarded. The precipitate was washed with PBS 1-2 times and diluted to equal OD (value of OD_{600} around 10 is better). 100 μl of diluted solution was taken and further dissolved using 400 μl of precipitant (80% methanol/acetonitrile + 20% water), the mixture was vortexed for 5 min and then put into liquid nitrogen to freeze for 5 min. The mixture was then put in -80 °C environment for 4 h and then centrifuged at 4 °C for 3 min. Finally, the supernatant was taken to test. Test and standard samples were injected in the liquid mass spectrometer and data was collected.

3. Results

3.1. Design and construction of independent modules for cell size tunning and HA synthesis

As stated in the introduction, FtsZ, encoded by one of the most important and widely studied morphology genes, is a cytokinesis protein that affects cell morphology by influencing the formation of Z-ring during cell division. In this study, when gene *ftsZ* was overexpressed under the strong inducible promoter P_{tac}, cell length and membrane area increased 4.8-fold and 5.2-fold respectively, compared to the wild type. The number of cells under iso-OD, however, plummeted to 1/16, resulting in a severe reduction of HA production, which decreased 75%. That is, a 5-fold enlargement is excessive for the cell, and under excessive deformation cell division was severely affected, thus reducing cell density and total HA production. In order to adequately control cell size and achieve enhancement in both high-density cell culture and high-titer HA production, we designed three independently functioning regulatory modules, namely the transporter module, the morphology tuning module and the HA synthesis module, where the first two modules are jointly responsible for cell size regulation and the last one is responsible for HA production (Fig. 1). By doing so we created a fine-tuning strategy for cell size completely independent of HA synthesis through adopting a strong constitutive promoter-weak inducible promoter composite, which is described as a dual-valve regulation as it can be tuned into different strengths to suit various needs.

For the morphology tuning module, since the strong promoter P_{tac}

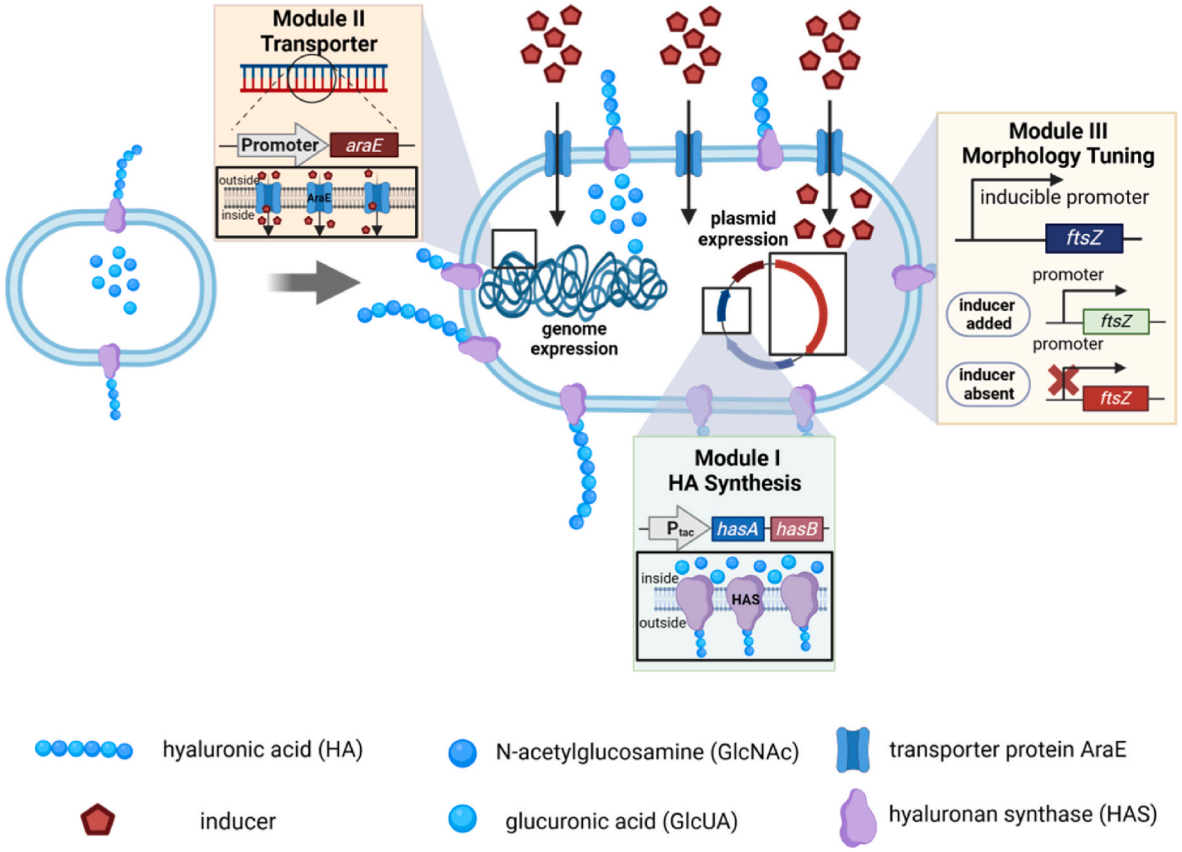

Fig. 1. Design of the three modules for fine-tunning the cell morphology together with HA synthesis. Module I, responsible for HA synthesis, expresses the HA synthesis operon (*hasA-hasB*) via strong inducible promoter P_{tac}. Module II, the transporter module, expresses the arabinose transporter gene *araE*, which will be driven by a constitutive strong promoter. Module III, the morphology tuning module, expresses the cell-division-relevant gene *ftsZ*, which will be driven by an inducible moderate-weak promoter. Draw with BioRender.com.

resulted in excessive deformation, a moderate or weak inducible promoter is preferred to attain a mild and independent tuning of cell size. First, the inducible promoters available in *C. glutamicum* were explored. With P_{tac} as control, a theoretical analysis based on the strength and induction mechanism of five commonly used inducible promoters in *C. glutamicum* was conducted. The studied promoters were β-isopropylthiogalactoside (IPTG)-inducible P_{trc}, arabinose-inducible P_{BAD}, tetracycline-inducible P_{tet}, rhamnose-inducible P_{rha} and cumate-inducible P_{cumate} (Fig. 2A). The inducer can enter the cell directly or through transporter proteins, for the latter, a controllable and accurate dual regulation for both the expression of the transporter protein and the concentration of inducer can be achieved. Hence, P_{tet} and P_{cumate}, which are both free of transporter protein in their inducible expression, lacking the demanded characteristics for designed dual-valve regulation for morphology gene to achieve more controllable and precise cell size change,[28,29] were not further considered. At the same time, P_{rha} was also not considered given its limited applications caused by the risk of severe leakage and its low expression intensity.[30] Lastly, P_{trc}, which shares the same inducer as P_{tac}, was also excluded.[31–33] Eventually, under comprehensive consideration of the induction mechanism and expression intensity, the moderate inducible promoter P_{BAD} was selected to accomplish both moderate cell size regulation and HA-enhanced accumulation.

The arabinose operon includes two promoters, P_c and P_{BAD}, a transcriptional regulatory protein, AraC, and three binding sites. When arabinose is not present, the AraC protein binds to the repression sites and the target gene regulated by this system will not be expressed. Contrary, when arabinose is present, it binds with the AraC protein, forming a complex binding to the excitation site and stimulate the expression of target gene. The composition and mechanism of arabinose operon is shown in Fig. S1.

For the transporter module, arabinose enters the cell with the help of the transporter protein AraE, which is absent in our host strain *C. glutamicum* ATCC13032.[34,35] To stabilize genetic circuits that regulate cell morphology, a strong constitutive promoter was preferred to allow more inducer to enter the cell. In contrast to the morphology module, in which the design was expressed on a plasmid, the transporter module was designed to directly integrate on the genome. Therefore, a range of endogenous promoters in *C. glutamicum* (Fig. 2B) were compared in terms of the GFP expression intensity, and the strong endogenous promoter P_{tuf} was selected to express the arabinose transporter protein AraE. When the gene *ftsZ* was expressed by P_{tac}, the resulting cell size was approximately 5-fold larger, but as the strength of P_{tuf} is about half of P_{tac}, we expect the maximum cell size to be about 2-fold larger, thus achieving a more suitable enlargement. Promoter P_{tuf} and gene *araE* were integrated on the genome by homologous recombination to construct the host strain Cg-P_{tuf}-araE, which is capable of transporting arabinose. Detailed information for the construction of Cg-P_{tuf}-araE is shown in Fig. S2.

Based on the above two modules, we elaborately designed a dual-valve strategy for cell size regulation. The transporter module served as the first valve for controlling the maximum amount of arabinose that can be transferred into cell, which corresponds to the maximum cell size change. Then the morphology tuning module expressing gene *ftsZ* using P_{BAD} served as the second valve for sensing intracellular inducer concentration and accordingly expressing *ftsZ* at different intensities, thus regulating changes in cell size. The opening of both valves, can be controlled by the expression levels of *araE* and *ftsZ*, respectively. By

(A)

Promoter	Inducer	Transporter protein for the inducer's entry	Expression intensity
P_{trc}	IPTG	+	*****
P_{BAD}	Arabinose	+	**
P_{tet}	Tetracycline	-	*
P_{rha}	Rhamnose	+	*
P_{cumate}	Cumate	-	***

(B)

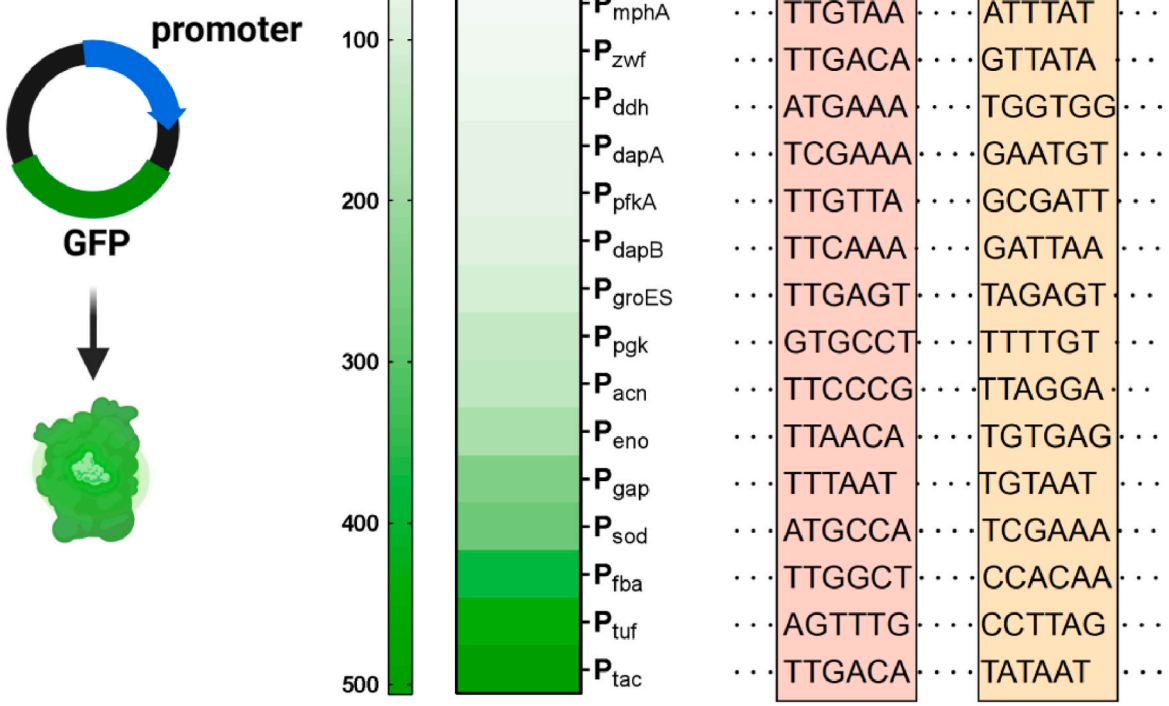

(C)

Strain name	Module I	Expression for module I	Module II	Expression for module II	Module III	Expression for module III
Cg01	+	P_{tac} hasA hasB	-		-	
Cg02	+	P_{tac} hasA hasB	+	P_{tac} ftsZ	+	P_{tuf} araE
Cg03	+	P_{tac} hasA hasB	+	P_{BAD} ftsZ	+	P_{tuf} araE

Fig. 2. Selection and construction of three strains based off the designed modules. (A) Comparison of commonly used inducible promoters in *C. glutamicum*, where + represents that transporter proteins are required for the entry of inducer into cell and - represents that transporter proteins are not required. * indicates the expression intensity of induction, the more * there are, the stronger expression intensity. (B) Comparison of endogenous promoter strengths and the -35 and -10 regions of *C. glutamicum*, where the intensity of green indicates the relative strength of the promoter. GFP, green fluorescence protein. -35 and -10 region was predicted by BPROM, http://www.softberry.com. (C) Construction of Cg01, Cg02 and Cg03. Expression of module I and II was on the plasmid while expression of module III was on the genome.

jointly regulating these two valves, cell size was expected to be enlarged to up to 2-fold, and different inducer concentrations were expected to aid achieving different levels of cell enlargement, thus creating a precise tuning method for cell size control.

For the HA synthesis module, the HA synthesis gene cluster (hyaluronan synthases, hasA and UDP-glucose dehydrogenase, hasB) was express by P_{tac} to maximize HA synthesis. Furthermore, to reduce additional introduction of plasmids which might affect stable copy for target gene, the HA synthesis gene cluster was expressed on the same plasmid along with the morphology gene *ftsZ*.

Hitherto, the three modules have been successfully defined and constructed. Additionally, to investigate the effect of cell size engineering on HA synthesis, we constructed a strain that did not undergo metamorphosis, Cg01, and two strains that contained the different cell size regulation modules, Cg02 and Cg03. The detailed information for these three strains is shown in Fig. 2C. In Cg02 HA module I and II was coupled as HA synthesis gene cluster and *ftsZ* were both expressed by strong inducible promoter P_{tac}. In Cg03, which is our target, the expression of HA synthesis gene cluster and *ftsZ* was separately controlled by P_{tac} and P_{BAD}. And cell size was regulated under the designed dual-valve regulation system which was composed of module II and module III via a strong constitutive promoter-weak inducible promoter composite. The construction and validation of these strains are shown in Fig. S3.

3.2. Cell size regulation of Cg01, Cg02 and Cg03

The optimal arabinose concentration for Cg03 was determined first by measuring OD_{600} and then by observing the change of cell size under different inducer concentrations (Fig. S4). Results indicated that 0.3 wt % was the optimal arabinose concentration. Also, the largest cell in the field of view was pictured and measured. It was found that under different arabinose concentration, the enlargement for cell size was different (Fig. 3). In the absence of inducer, cell size remained unchanged compared to the wild type, meaning that the leakage expression level of the dual-valve regulation system is extremely low. In contrast, with the increase of inducer concentration, cell size showed a trend of increasing, remaining stagnant and finally decreasing. Results showed that the maximum enlargement was under concentration of 0.4 wt%, meaning 2.8 μm in cell size. Under concentration of 0.3 wt% cell size enlarged 2-fold compared with the control, which perfectly fit with our expectation. It also verified the ability of the dual-valve system to cause change in cell size to up to 2-fold depending on the inducer concentration, thus providing insight into achieving controllable and fine tuning for cell size.

The structure of the division protein FtsZ plays a crucial role in the morphology tuning module. As FtsZ protein structure in *C. glutamicum* is not reported, its structure was predicted (Fig. 4A). Through qRT-PCR, the transcription level of the gene *ftsZ* was observed. It was found that expression of *ftsZ* in Cg03 using P_{BAD} under regulation of the dual-valve system was 10-fold higher compared to Cg01. Replacing P_{BAD} with P_{tac}, the expression level of *ftsZ* reached about 300-fold higher (Fig. 4B), consequently verifying that the appropriate expression of the morphology gene was favored by regulation of the dual-valve system. Finally, the melt curves for three parallel samples during qRT-PCR (Fig. 4C) almost completely overlapped and each showed a single peak, indicating that the results in Fig. 4B are high-accurate.

Cell deformation was consistent with the results of the *ftsZ* relative expression level, as shown by the scanning electron microscope and transmission electron microscope images in Fig. 5A and B. With Cg01 as control, results show that Cg02 produced significant deformation, which was about 5-fold increase in cell length, whereas deformation of Cg03 was relatively more modest, with an approximate 2-fold increase in cell length, that being 2-3 μm. Multiple fields of view for one sample were photographed and the accurate cell length was obtained by scale conversion, photographs of the longest cells were then taken and used to show how the conversion was done (Fig. 5C). 130 cells were counted in each strain sample, from which we calculated the average cell length and average membrane area (Table 3) and depicted their distributions in Fig. 5D and E. Results showed that both the average and maximum cell

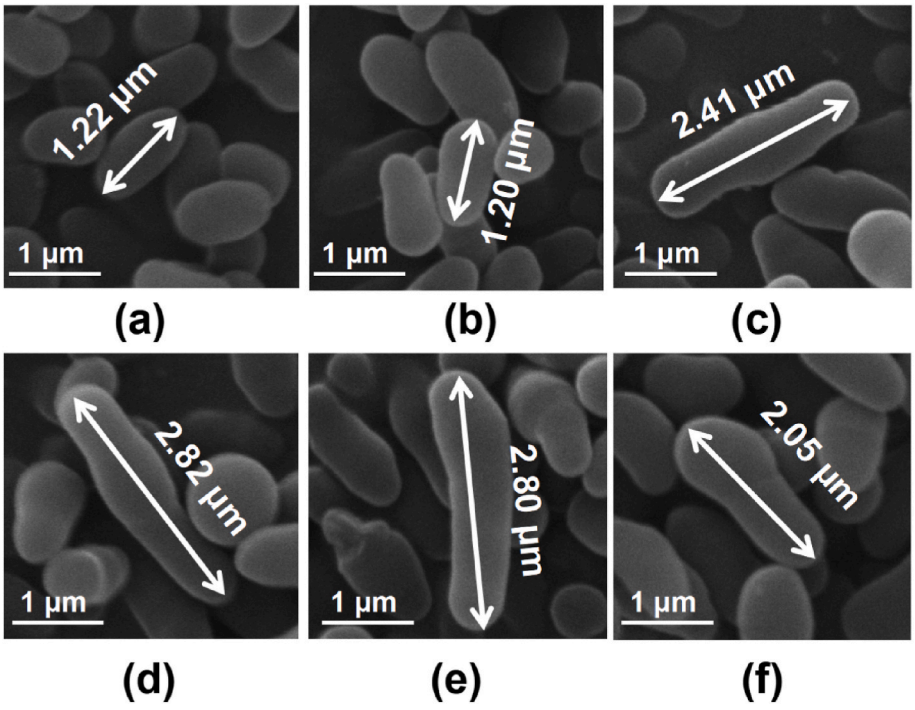

Fig. 3. Scanning electron microscope images of the largest cell in wild type and Cg03 under different concentrations, respectively. Cg03 contains plasmid pEC-P_{tac}-AB-P_{BAD}-*ftsZ*. The inducer IPTG concentration was 0.3 mM and the arabinose concentration was 0.3 wt%. (a) wild type *C. glutamicum* ATCC13032, (b) 0 wt% arabinose, (c) 0.3 wt% arabinose, (d) 0.4 wt% arabinose, (e) 1 wt% arabinose, (f) 2 wt% arabinose. All images and cell length measurements were done at uniform scale.

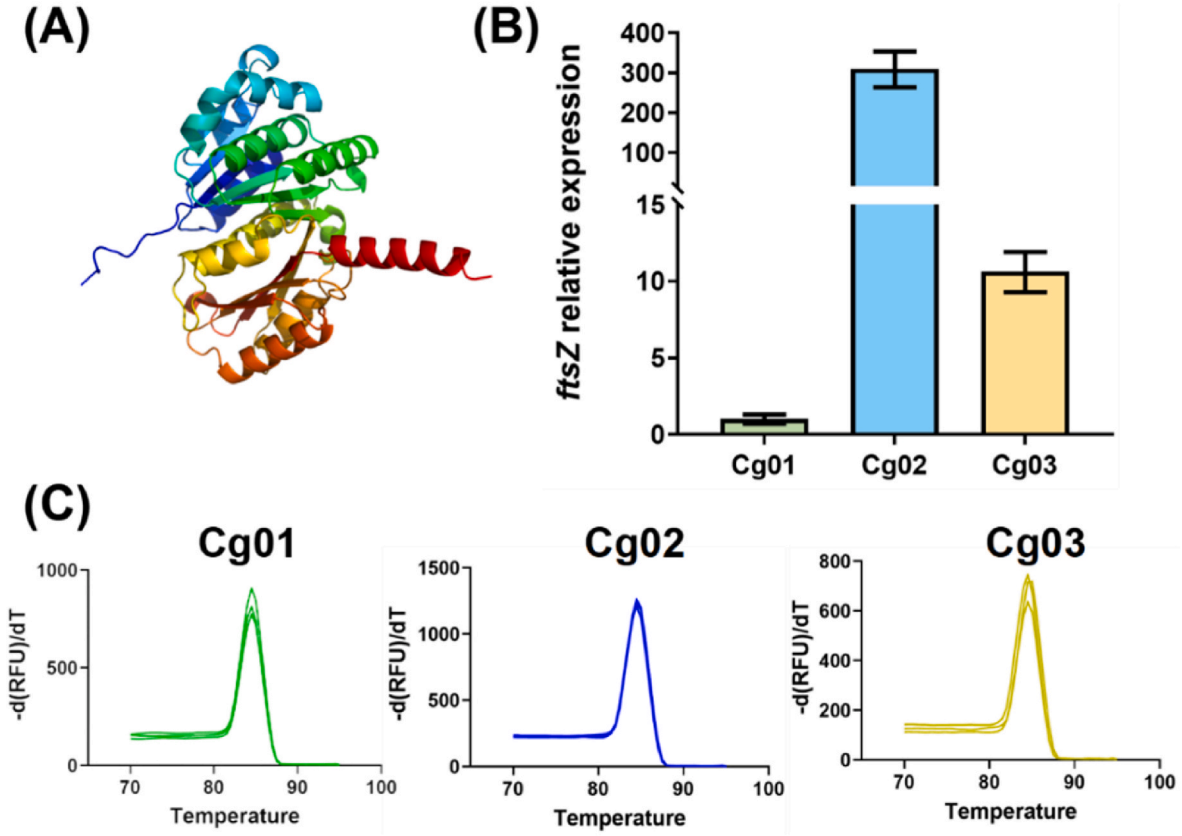

Fig. 4. Results for quantitative real-time PCR for Cg01, Cg02 and Cg03, where Cg01 contained plasmid pEC-P_{tac}-AB, Cg02 contained plasmid pEC-P_{tac}-AB-*ftsZ*, and Cg03 contained plasmid pEC-P_{tac}-AB-P_{BAD}-*ftsZ*. The IPTG inducer concentration was 0.3 mM and the arabinose concentration was 0.3 wt%. (A) Structure for protein FtsZ in *C. glutamicum*, predicted by AlphaFold, https://www.alphafold.ebi.ac.uk/. (B) Relative expression level of the gene *ftsZ* in 24 h for the three recombinant strains. Experiments were reproduced in triplicate. (C) Melt curves of the three parallel samples.

length in Cg03 were about a 2-fold enlargement, with average of 2.54 μm and maximum of 4.3 μm. The average cell membrane area also increased 2-fold, which was around 7.47 μm^2, while the maximum membrane area reached 2.8-fold, which was 14.2 μm^2. Enlargement of cell size in Cg02 was more remarkable, reaching about 4-fold in both average cell length and membrane area, which were 4.41 μm and 11.93 μm^2, respectively. And the maximum cell membrane area increased around 12-fold reaching 60.5 μm^2. From Fig. 5D and E, it was found that cell size distribution including cell length and membrane area was the most concentrated in Cg01, followed by Cg03, with Cg02 having the widest cell size distribution. It suggested that cell sizes are not identical, rather they are distributed within a range of values and cell deformation affects the distribution of cell sizes. Compared with Cg02, Cg03 has less effect on cell size distribution, which further illustrates the superiority of dual-valve regulation strategy.

3.3. Cell number and HA synthesis in recombinant C.glutamicum

When cells undergo metamorphosis, the linear relationship between OD_{600} and the number of cells cannot be deduced since larger cells absorb more light compared to normal cells, yet cell size was not accounted as a variable in the relationship. Thus, an alternative method to characterize cell density and growth according to the cell count using optical microscope and transmission electron microscope was used. It was found by TEM imagery that under same dilution level cell count in Cg03 was significantly higher than that in Cg01 and Cg02 (Fig. 6A). Hemocyte counting plates were used to count the number of cells per OD_{600} under iso-OD condition. When observing cell density in one counting square under optical microscope, it was found that cell density for Cg02 was significantly lower than Cg03, which did not deviate much from Cg01 (Fig. 6B). The results are consistent with literature, a dramatic decrease in cell number occurred when *ftsZ* was overexpressed using P_{tac}. OD_{600} was measured using a spectrophotometer, through which the cell number per OD_{600} was calculated (Fig. S5), allowing for an assessment over the total cell count (Fig. 6C). Because of excessive cell deformation, the cell counts in Cg02 decreased about 33% compared to the control group despite the invariant value of OD_{600}. In contrast, the effect of deformation on the cell count of Cg03 was almost negligible. Essentially, the total cell count of *C.glutamicum* under the dual-valve regulation system showed little deviation from the control group, meaning the dual-valve regulation system does not affect cell growth.

Without altering the expression of HAS, it can be inferred that the improvement of HA production in Cg03 is caused by the increase in cell membrane area leading to additional attachment sites for HAS, thus improving the efficiency of HA synthesis. The ability of HA synthesis in Cg03 was indirectly illustrated by measuring the concentration of metabolites on the HA synthesis pathway. Results showed that the concentration of two reaction precursors, UDP-GlcUA and UDP-GlcNAc, were both reduced in Cg03 compared with the control strain Cg01, indicating an increase in the amount of these precursors being used by HAS to produce HA (Fig. 7A). Moreover, no significant changes were found for the concentration of other metabolites in HA synthesis pathway, further indicating that cell size engineering did not alter pathways other than the HA synthesis reaction. The ability of single cells to synthesize HA was also enhanced following enlargements in membrane area leading to a theoretical increase in attachment sites for the membrane protein HAS. Both deformed recombinants of *C.glutamicum*, Cg02 and Cg03, showed better performance in single cell HA synthesis (Fig. 7B). A remarkable increase of single cell HA synthesis of about 3-fold was achieved by Cg02. Excessive deformation caused a significant

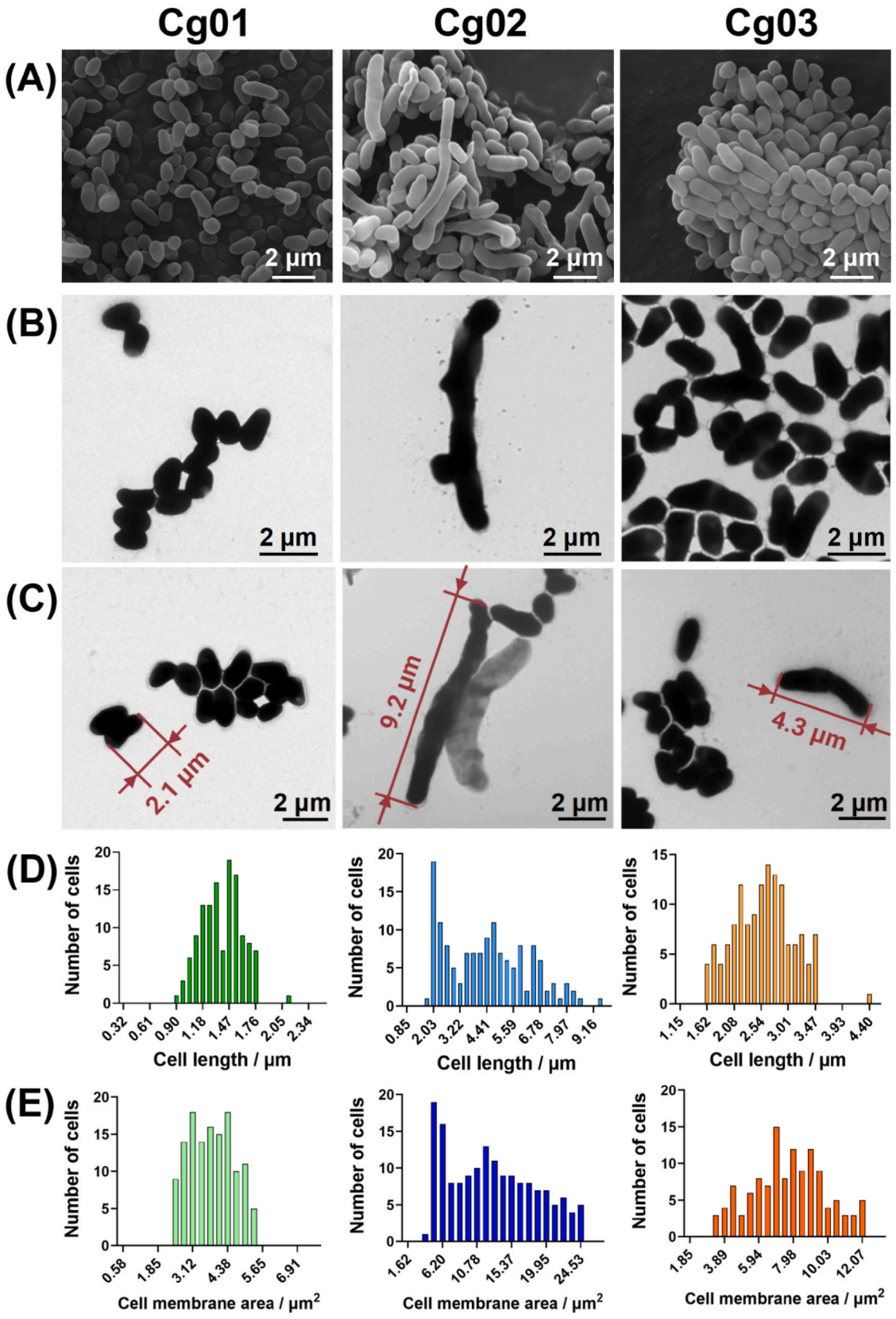

Fig. 5. Results for cell deformation for Cg01, Cg02 and Cg03. The inducer IPTG concentration was 0.3 mM and the arabinose concentration was 0.3 wt%. (A) Scanning electron microscope images of the three recombinant strains. (B) Transmission electron microscope images of the three recombinant strains. (C) The longest cell in the view field and measurement for acurate cell length. (D) Distribution of cell length in the three recombinant strains. (E) Distribution of cell membrane in the three recombinant strains.

Table 3
The statistics cell length and membrane area of three recombinant strains.

	Cg01	Cg02	Cg03
Maximum cell length/μm	2.1	9.2	4.3
Increase fold	/	4.4	2.0
Averag cell length/μm	1.36 ± 0.21	4.41 ± 1.98	2.54 ± 0.46
Increase fold	/	3.2	1.9
Maximum membrane area/μm^2	5.1	60.5	14.2
Increase fold	/	11.9	2.8
Average membrane area/μm^2	3.59 ± 0.75	11.93 ± 4.76	7.47 ± 2.04
Increase fold	/	3.3	2.1

Note: The inducer IPTG concentration was 0.3 mM and the arabinose concentration was 0.3 wt%. The length and diameter parameters of single cells were estimated by microscopic observation. 130 cells for each strain were randomly selected and observed to calculate the mean value of the length and diameter.

increase in single cell HA synthesis but also a counterproductive decrease in cell number causing the HA titer to plummet (Fig. 7C). Cg03 showed a slight increase in single-cell HA titer, coupled with a remarkable increase in cell count, which resulted in increased HA titer of 16.0 g/L, which was 1.6-time compared with Cg02, conclusively showing the significance of controllable and fine tuning via the dual-valve strategy. Hence, for the first time, a morphologically engineered strain resulting in both high cell density and HA titer was constructed. Moreover, compared with Cg01, single cell HA synthesis was also enhanced using this strategy, leading to a 1.2-fold increase in HA titer.

Comprehensively, cell size regulation via dual-valve strategy comprised with the morphology tuning module and the transporter module showed great enhancement on single cell HA synthesis and improvement on HA titer, achieving high cell density and high HA titer in *C.glutamicum*.

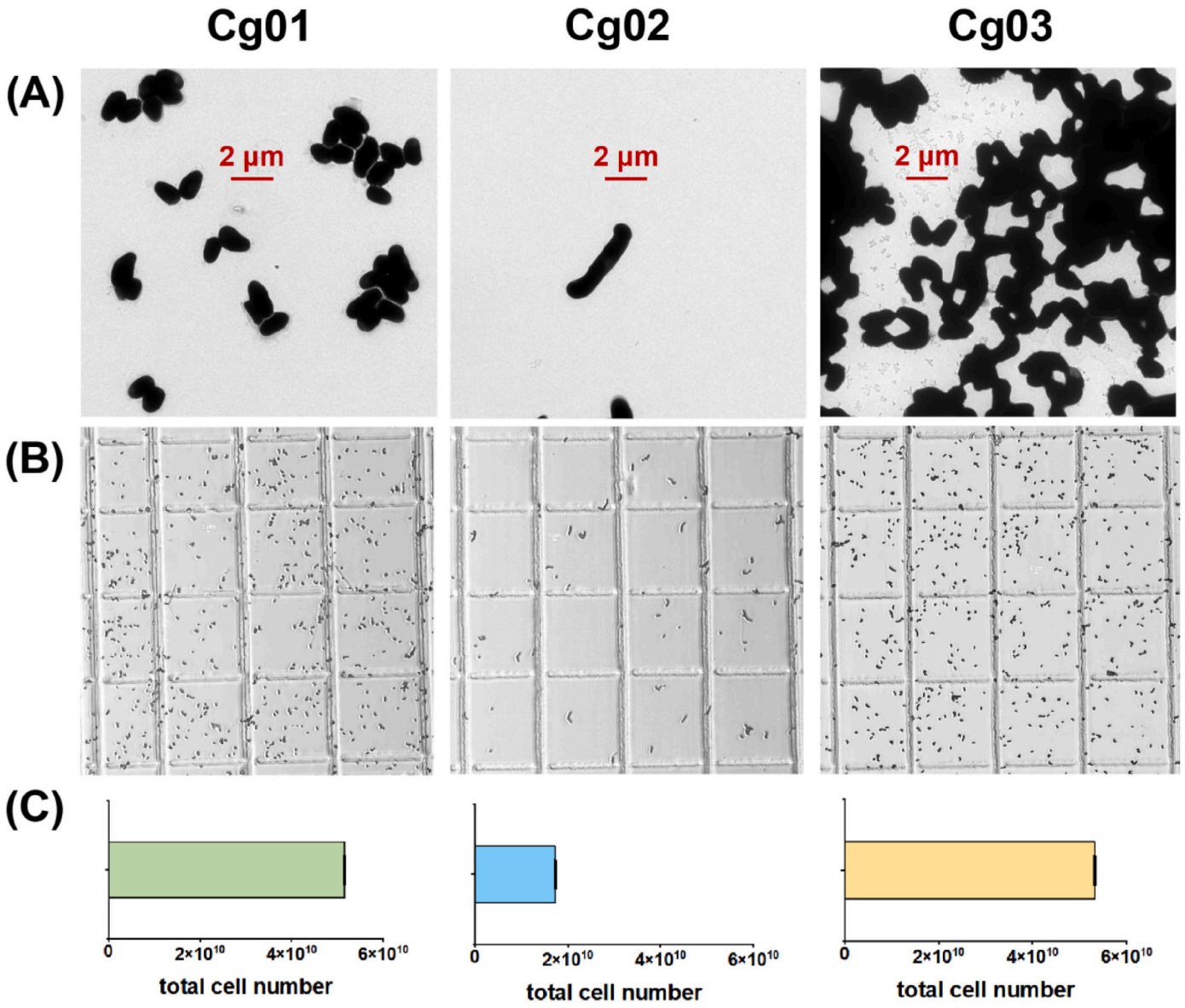

Fig. 6. Comparison of cell number for Cg01, Cg02 and Cg03, where Cg01 contains plasmid pEC-P_{tac}-AB, Cg02 contains plasmid pEC-P_{tac}-AB-*ftsZ*, Cg03 contains plasmid pEC-P_{tac}-AB-P_{BAD}-*ftsZ*. The inducer IPTG concentration was 0.3 mM and the arabinose concentration was 0.3 wt%. (A) Transmission electron microscope imagery at the same magnification. All three tested samples were diluted 20 times. (B) Optical microscope photograph of a counting unit on the hemocyte counting plate. All three tested samples were dilute to OD_{600} of 1. (C) Total cell number in 1 mL fermentation broth calculated using hemocyte counting plates. Experiments were reproduced in duplicate.

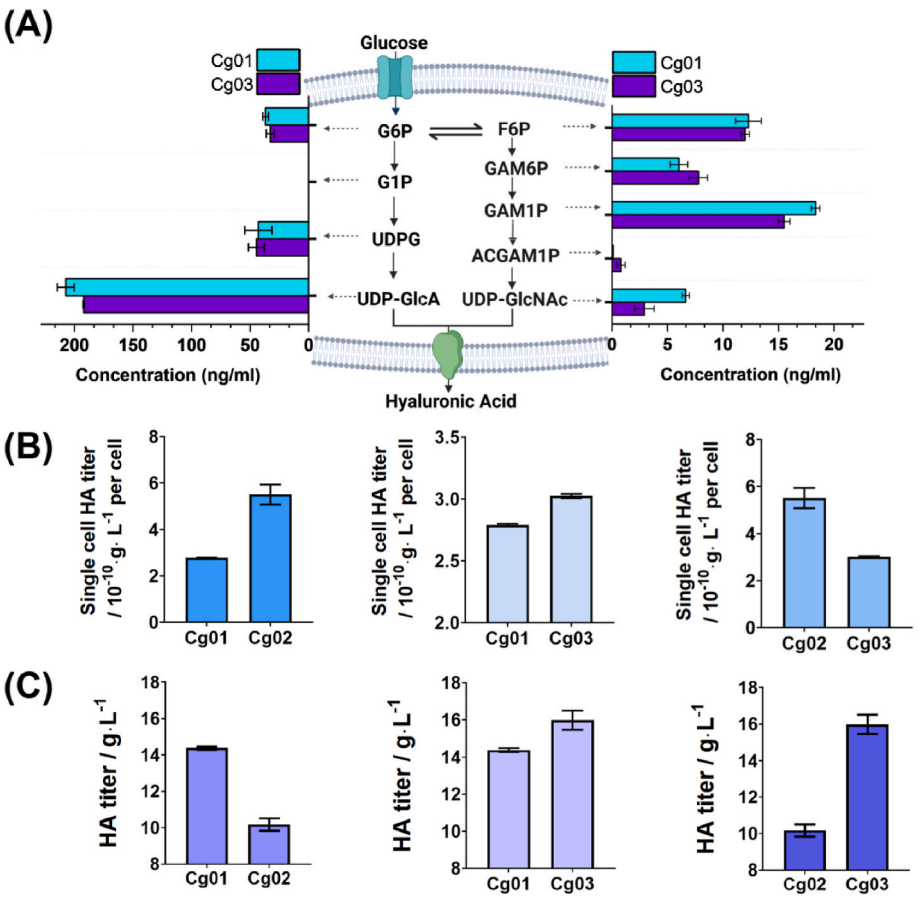

Fig. 7. HA synthesis in shake flask culture for Cg01, Cg02 and Cg03, where Cg01 contains plasmid pEC-P_{tac}-AB, Cg02 contains plasmid pEC-P_{tac}-AB-*ftsZ*, Cg03 contains plasmid pEC-P_{tac}-AB-P_{BAD}-*ftsZ*. The inducer IPTG concentration was 0.3 mM and the arabinose concentration was 0.3 wt%. (A) Quantification results of metabolites in HA synthesis pathway. The blue bar is the result for Cg01 and purple bar is the result for Cg03.Experiments were reproduced in triplicate. Metabolites were depicted in capital letters. G6P: glucose-6-phosphate; G1P: glucose-1-phosphate; UDPG: UDP-glucose; UDP-GlcA: UDP glucuronate; F6P: fructose-6-phosphate; GAM6P: glucosamine-6-phosphate; GAM1P: glucosamine-1-phosphate; ACGAM1P: N-acetyl-glucosamine-1-phosphate; UDP GlcNAc: UDP-N-acetyl-glucosamine. (B) Comparison of single-cell HA synthesis at 48 h between Cg01, Cg02 and Cg03. (C) Comparison of HA titer at 48 h between Cg01, Cg02 and Cg03.The inducer IPTG concentration and arabinose concentration was 0.3 mM and 0.3 wt%, respectively. Experiments were reproduced in triplicate. Draw with BioRender.com.

4. Discussion

HA has significant application values in the fields of medicine, cosmetics and health care products, thus overcoming the bottleneck of HA synthesis has tremendous market value. Previous attempts to strengthen HA synthesis through cell size enlargement were discontinued after achieving single-cell level enhancements since excessively deformation led to obstruction of normal cell growth. Discouraged by the plummet in overall HA production, further applications of cell size engineering in HA production were no longer studied.[23] This work provides a methodical solution to the problem, balancing the effects of deformation on cell growth and product yield. In previous works of our laboratory team, the HA titer of metabolically engineered strains achieved about 8 g/L in shake flask at 48 h and 32 g/L in 10 L fermenter at 60 h. Through the application of cell size engineering, the strain constructed in this work, Cg03, was able to reach shake flask titer of 16 g/L at 48 h, which is 1.6-time than Cg02 and 2-time than the previous engineered strains. Thus, providing insight for improving the performance of HA synthesis at fermenter level to meet industrial needs.

In addition to metabolic pathway optimization and modification, cell size engineering is also recognized as a novel approach to effectively construct various cell factories. Morphology engineering has been widely used in the production of poly-β-hydroxybutyrate (PHB), which generated remarkable results. As reported in literature, the overexpression of gene *sulA* in *E. coli* inhibited the formation of Z-rings during cell division, resulting in the formation of elongated cells that provided more space for intracellular accumulation of PHB, doubling PHB accumulation to 2.19 g/L,[36] showing that the accumulation of intracellular products is proportional to the cell volume.[37] For extracellular products, deformation tends to affect cell growth and is detrimental to product synthesis. In a previous work reporting the synthesis of extracellular product alginate oligosaccharides (AOs), overexpression of MreB in *Pseudomas mendocina* resulted in a 1.27-fold and 1.49-fold increase in cell length and width respectively, while overexpression of MreB made cell growth slow.[38] Thus, morphology engineering proves to be an innovative approach to optimize and control the physical characteristics and structure of microorganisms, offering significant advantages in improving the process flexibility of efficient production of valuable products.

Cell size plays a crucial role in influencing the accumulation of intracellular products and the secretion of extracellular product, thus it is important to develop a fine-tuning method for the precise regulation of cell size. The dual-valve regulation system in this study, based on an arabinose-inducible promoter strategically developed through the construction of the transporter module and the morphology tuning module, has the potential to be applied to the cell size regulation of other strains and to enhance the synthesis of other target products. This dual-valve system works by a facile adjustment of the inducer concentration, which can increase the average length and membrane area of cells to up to two times the original scale. More importantly, this novel system can

effectively avoid excessive cell deformation, allowing for normal cell growth and division. Here, we successfully accomplished fine-tuning of cell size of *C. glutamicum* and applied this practical strain to enhance HA synthesis by increasing the maximum length and membrane area of cells by 1.87-fold and 2.08-fold respectively, setting a threshold for cell size enlargement.

The method developed in this work can be further combined with other strategies to collaboratively achieve hyper-production of HA. For example, as extracellular capsule-like layer may further increase the inhibition for metabolism and resistance for mass transfer due to cell enlargement, coupling with hyaluronidase addition strategy has great potential to improve low molecular weight HA yield.[12] Cardiolipin is an important cofactor for maintaining HAS activity, so enhancing cardiolipin synthesis can increase HAS activity and HA production.[11] Westbrook et al. strengthened cardiolipin synthesis while overexpressed gene *ftsZ* to enlarge the cells size in *B. subtilis*, changing the distribution of cardiolipin in the lateral membranes, which in turn enhanced the interaction between cardiolipin and HAS, enhanced the activity of HAS and increased the HA production by 204%.[22] Therefore, cardiolipin overexpression coupled with fine-tuning cell size of *C.glutamicum* in this work will further strengthen HA synthesis, which will generate great potential for HA productivity enhancing and new product development in the future.

To conclude, this work focuses on the precise tuning of cell morphology to increase the levels and activity of the crucial protein HAS through the construction of a novel dual-valve system able to achieve precise regulation of cell morphology leading to enhanced HA production.

Declaration of competing interest

Huimin Yu is an Associate Editor for Biotechnology Notes and was not involved in the editorial review or the decision to publish this article. All authors declare that the research was conducted in the absence of any commercial or financial relationships that could be construed as a potential conflict of interest.

Acknowledgement

This work was supported by the National Key R&D Program of China (2021YFC2103100), Shandong Province Key R&D Program of China (2020CXGC010602) and Natural Science Foundation of China (No. 22078173).

Appendix A. Supplementary data

Supplementary data to this article can be found online at https://doi.org/10.1016/j.biotno.2023.12.003.

References

1. Zheng X, Wang B, Tang X, et al. Absorption, metabolism, and functions of hyaluronic acid and its therapeutic prospects in combination with microorganisms: a review. *Carbohydrate Polym*. 2023;299.
2. Liu L, Liu Y, Li J, et al. Microbial production of hyaluronic acid: current state, challenges, and perspectives. *Microb Cell Factories*. 2011;10:99.
3. Kobayashi T, Chanmee T, Itano N. Hyaluronan: metabolism and function. *Biomolecules*. 2020;10(11).
4. Gunasekaran V, G D, P V. Role of membrane proteins in bacterial synthesis of hyaluronic acid and their potential in industrial production. *Int J Biol Macromol*. 2020;164:1916–1926.
5. Schulte S, Doss SS, Jeeva P, et al. Exploiting the diversity of streptococcal hyaluronan synthases for the production of molecular weight–tailored hyaluronan. *Appl Microbiol Biotechnol*. 2019;103(18):7567–7581.
6. Yu H, Stephanopoulos G. Metabolic engineering of Escherichia coli for biosynthesis of hyaluronic acid. *Metab Eng*. 2008;10(1):24–32.
7. Mao Z, Shin H-D, Chen R. A recombinant E. coli bioprocess for hyaluronan synthesis. *Appl Microbiol Biotechnol*. 2009;84(1):63–69.
8. Jin P, Kang Z, Yuan P, et al. Production of specific-molecular-weight hyaluronan by metabolically engineered Bacillus subtilis 168. *Metab Eng*. 2016;35:21–30.
9. Jia Y, Zhu J, Chen X, et al. Metabolic engineering of Bacillus subtilis for the efficient biosynthesis of uniform hyaluronic acid with controlled molecular weights. *Bioresour Technol*. 2013;132:427–431.
10. Cheng F, Yu H, Stephanopoulos G. Engineering Corynebacterium glutamicum for high-titer biosynthesis of hyaluronic acid. *Metab Eng*. 2019;55:276–289.
11. Du Y, Cheng F, Wang M, et al. Indirect pathway metabolic engineering strategies for enhanced biosynthesis of hyaluronic acid in engineered Corynebacterium glutamicum. *Front Bioeng Biotechnol*. 2021;9.
12. Wang Y, Hu L, Huang H, et al. Eliminating the capsule-like layer to promote glucose uptake for hyaluronan production by engineered Corynebacterium glutamicum. *Nat Commun*. 2020;11(1).
13. Chien L-J, Lee C-K. Hyaluronic acid production by recombinant Lactococcus lactis. *Appl Microbiol Biotechnol*. 2007;77(2):339–346.
14. Sunguroğlu C, Sezgin DE, Aytar Çelik P, et al. Higher titer hyaluronic acid production in recombinantLactococcus lactis. *Prep Biochem Biotechnol*. 2018;48(8):734–742.
15. Yao Z-Y, Qin J, Gong J-S, et al. Versatile strategies for bioproduction of hyaluronic acid driven by synthetic biology. *Carbohydrate Polym*. 2021:264.
16. Manfrão-Netto JHC, Queiroz EB, Oliveira Junqueira AC, et al. Genetic strategies for improving hyaluronic acid production in recombinant bacterial culture. *J Appl Microbiol*. 2021;132(2):822–840.
17. Vigetti D, Viola M, Karousou E, et al. Metabolic control of hyaluronan synthases. *Matrix Biol*. 2014;35:8–13.
18. Guo L, Pang Z, Gao C, et al. Engineering microbial cell morphology and membrane homeostasis toward industrial applications. *Curr Opin Biotechnol*. 2020;66:18–26.
19. Jiang X-R, Chen G-Q. Morphology engineering of bacteria for bio-production. *Biotechnol Adv*. 2016;34(4):435–440.
20. Huo K, Zhao F, Zhang F, et al. Morphology engineering: a new strategy to construct microbial cell factories. *World J Microbiol Biotechnol*. 2020;36(9).
21. Jiang X-R, Wang H, Shen R, et al. Engineering the bacterial shapes for enhanced inclusion bodies accumulation. *Metab Eng*. 2015;29:227–237.
22. Westbrook AW, Ren X, Moo-Young M, et al. Engineering of cell membrane to enhance heterologous production of hyaluronic acid in Bacillus subtilis. *Biotechnol Bioeng*. 2017;115(1):216–231.
23. Zheng Y, Cheng F, Zheng B, et al. Enhancing single-cell hyaluronic acid biosynthesis by microbial morphology engineering. *Synthetic and Systems Biotechnology*. 2020;5(4):316–323.
24. Yang P, Liu W, Cheng X, et al. A new strategy for production of 5-aminolevulinic acid in recombinant Corynebacterium glutamicum with high yield. *Appl Environ Microbiol*. 2016;82(9):2709–2717.
25. Cheng F, Luozhong S, Guo Z, et al. Enhanced biosynthesis of hyaluronic acid using engineered Corynebacterium glutamicum via metabolic pathway regulation. *Biotechnol J*. 2017;12(10).
26. Cheng F, Gong Q, Yu H, et al. High-titer biosynthesis of hyaluronic acid by recombinant Corynebacterium glutamicum. *Biotechnol J*. 2016;11(4):574–584.
27. Cheng F, Luozhong S, Yu H, et al. Biosynthesis of chondroitin in engineered Corynebacterium glutamicum. *J Microbiol Biotechnol*. 2019;29(3):392–400.
28. Lausberg F, Chattopadhyay AR, Heyer A, et al. A tetracycline inducible expression vector for Corynebacterium glutamicum allowing tightly regulable gene expression. *Plasmid*. 2012;68(2):142–147.
29. Seo S-O, Schmidt-Dannert C. Development of a synthetic cumate-inducible gene expression system for Bacillus. *Appl Microbiol Biotechnol*. 2018;103(1):303–313.
30. Hogan A, Jeffers K, Palacios A, et al. Improved dynamic range of a rhamnose-inducible promoter for gene expression in burkholderia spp. *Appl Environ Microbiol*. 2021;87(18), e00647, 21.
31. Tsuchiya M, Morinaga Y. Genetic control systems of ESCHERICHIA coli can confer inducible expression of cloned genes in coryneform bacteria. *Biotechnology*. 1988;6.
32. Teramoto H, Inui M, Yukawa H. Transcriptional regulators of multiple genes involved in carbon metabolism in Corynebacterium glutamicum. *J Biotechnol*. 2011;154(2-3):114–125.
33. Henke NA, Krahn I, Wendisch VF. Improved plasmid-based inducible and constitutive gene expression in Corynebacterium glutamicum. *Microorganisms*. 2021;9(1).
34. Khlebnikov A, Risa Ø, Skaug T, et al. Regulatable arabinose-inducible gene expression system with consistent control in all cells of a culture. *American Society for Microbiology*. 2000;182(24):7029–7034.
35. Zhang Y, Shang X, Lai S, et al. Development and application of an arabinose-inducible expression system by facilitating inducer uptake in Corynebacterium glutamicum. *Appl Environ Microbiol*. 2012;78(16):5831–5838.
36. Wang Y, Wu H, Jiang X, et al. Engineering Escherichia coli for enhanced production of poly(3-hydroxybutyrate-co-4-hydroxybutyrate) in larger cellular space. *Metab Eng*. 2014;25:183–193.
37. Elhadi D, Lv L, Jiang X-R, et al. CRISPRi engineering E. coli for morphology diversification. *Metab Eng*. 2016;38:358–369.
38. Fan X, Gong T, Wu Y, et al. Enhanced synthesis of alginate oligosaccharides in Pseudomonas mendocina NK-01 by overexpressing MreB. *3 Biotech*. 2019;9(9).